

Monitoring the post Construction Structural and Environmental behaviours of an Instrumented Smart Pavement Section

Matea Ceric, MASc Candidate, Department of Civil and Environmental Engineering, University of Waterloo

Abimbola Grace Oyeyi, Post-Doctoral Fellow, Department of Civil and Environmental Engineering, University of Waterloo

Shenglin Wang, Post-Doctoral Fellow, Department of Civil and Environmental Engineering, University of Waterloo

Pejooohan Tavassoti, Assistant Professor, Jr. Norman W. McLeod Chair in Sustainable Pavement Engineering, Department of Civil and Environmental Engineering, University of Waterloo

Hassan Baaj, Associate Chair for Research, Norman W. McLeod Chair in Sustainable Pavement Engineering, Department of Civil and Environmental Engineering, University of Waterloo

Omran Maadani, Associate Research Scientist, National Research Council of Canada

Mohammad Shafiee, Associate Researcher, National Research Council of Canada

Paper prepared for presentation at the “Innovations in Pavement Management, Engineering and Technologies” session of the 2023 TAC Conference & Exhibition, Ottawa, ON

Abstract

Pavement infrastructure worldwide is pivotal to successful economic growth. However, like all infrastructure, it requires proper Maintenance and Rehabilitation (M&R) strategies and evidence-based Pavement Management Systems (PMS) to ensure that the pavement condition can meet the desired level of service under the impact of traffic loads and given climatic loading parameters. With the improvement of new paving materials, climate change and extreme weather events impacts solely relying on traditional M&R techniques, where monitoring periods are scheduled sporadically, may not be enough to understand pavement's performance and their mechanistic response to varying loading and climatic conditions. However, pavement design and management can benefit from the concept of Smart Pavements, considering the recent advances in Artificial Intelligence (AI) and instrumentation monitoring systems. This study presents a summary of the current progress for the “smart pavements” concept currently being implemented within a section of a major two-lane arterial roadway in Kitchener, Ontario. The goal is to enable pseudo-real-time monitoring of the section and understand the actual in-situ responses through advanced instrumentation and by running Machine Learning models to improve our understanding and prediction of long-term pavement performance. Thus far, the installation and construction of the instrumented section have been completed, and preliminary results have been obtained. This paper presents the preliminary pavement environmental and structural behaviours immediately after the construction of the section, as well as five months after construction. The instrumentation installed in each layer consists of horizontal and vertical asphalt concrete strain gauges, moisture probes, pressure cells, and temperature strings. The impact of asphalt temperature right after construction until service condition and loading frequencies on the structural behaviors of the pilot section were monitored through several rounds of known weight axial truck. The results are used to establish a baseline for better interpretation of the pavement structure during its in-service monitoring period.

1.0 Introduction

Pavement infrastructure plays a crucial role in facilitating successful economic growth worldwide, including in countries like Canada (OECD, 2020). Like any other infrastructure, pavements require consistent maintenance and rehabilitation (M&R) strategies and pavement management systems (PMS) to ensure they can handle the desired traffic loads and adapt to the effects of climate change (Centre for Pavement and Transportation Technology, 2019; Amândio et al., 2021).

Traditional M&R techniques pose challenges due to their high costs and reliance on manual and destructive assessments, such as the falling-weight deflectometer (FWD), ground penetrating radar (GPR), borehole analysis, etc. (Benedetto & Pensa, 2007). Consequently, monitoring periods are not adequately scheduled for proper pavement maintenance (Amândio et al., 2021). These techniques also struggle to accurately measure pavement responses and in situ conditions, such as stresses, strains, and moisture variations throughout the year, at different pavement structure layers (Centre for Pavement and Transportation Technology, 2019).

However, recent advancements in artificial intelligence (AI) and sensory systems offer the potential for continuous pavement monitoring. This technological progress could result in cost savings, reduced material usage, increased efficiency, and improved understanding of pavement structures over time by enabling real-time pavement performance monitoring (Amândio et al., 2021).

Some previous and known examples of pavement instrumentation include the Virginia Smart Roads project, whereby sections of newly built test road were instrumented with pressure cells, strain gauges, moisture sensors and temperature sensors to be able to collect both load and environmental data related to the pavement test section (Al-Qadi et al., 2004). In France, Duong et al. (2018) also instrumented a pavement

test section deflection using geophones. In Canada, there have been previous examples of pavement instrumentation, such as that in Ottawa, Ontario, as described by Maadani et al. (2015).

Although much of the previous literature has focused on the results of the instrumented pavement test section and the impacts of load and/or climate on the evolution of pavement performance deterioration, there is still minimal research on the use of this data in actual pavement performance deterioration model using load and environmental data of embedded sensors. Typically, the literature has focused on the use of AI to identify surface distresses through image prediction (Hou et al., 2020; Amândio et al., 2021). In addition, the development of the performance prediction model, as well as the data gathered from all of the sensors, is set to contribute to the emerging research of “smart pavements”, whereby a variety of data is received from the pavement structure in the form of load, environmental impacts, energy generation, traffic counts, etc. to provide a wholistic state of the infrastructure.

Currently, this concept of an instrumented test section is being implemented in a segment of a major arterial roadway in Kitchener, Ontario, as part of a broader road reconstruction project. The objective is to enable pseudo-real-time monitoring of this section and gain insights into its in-situ responses by utilizing advanced instrumentation and running an AI model. The goal is to enhance the understanding and prediction of the section's long-term pavement performance.

To do this, some of the objectives include analyzing data obtained from a pavement test section at different traffic load levels, speeds, and temperatures and also providing an indication of the nature of pavement response to inform the development of AI predictive models.

2.0 Objectives and Scope

It is crucial to collect and comprehend relevant and precise data to develop an accurate AI model for predicting pavement performance deterioration over time and identifying critical impacts within the pavement structure layers. This data encompasses performance or load data (strain, pressure, and deflection) as well as environmental data (temperature and moisture). Consequently, a currently open road section was instrumented with a diverse range of sensors to capture this vital information. This paper provides a description of the sensor types and variety deployed in the instrumented pavement section.

Subsequently, the paper presents the results of two truck tests conducted: one during construction and another after five months of open traffic conditions. The analysis covers the effects of traffic loads on pressure and strain, the impact of temperature on pressure and strain, and finally, the influence of speed on pressure and strain. A comparative assessment was conducted between the conditions during construction, and those observed several months later under open traffic conditions.

3.0 Project Location and Instrumentation

The instrumented test section is located on Courtland Avenue East in Kitchener, Ontario. This road is classified as a Major Arterial roadway. It passes underneath Highway 8 while also being connected to several highway onramps and offramps. From Figure 1, the instrumented test section is situated between the intersections of Overland Drive and Courtland Avenue East, Walton Avenue and Courtland Avenue East, and is about 10 meters long. Figure 1 also showcases the test section location from a street-view perspective.



Figure 1 Location of Trial Section in relation to nearby roads and street view at approximate test section location (Google, 2023)

A range of sensors was deployed in the instrumented section to continuously gather information on the load-induced and environmental impacts on the pavement structure. These sensors encompass horizontal and vertical asphalt strain gauges, temperature sensors, moisture probes, multi-depth deflectometers (MDD), total earth pressure cells (TEPC), and temperature probes that measure temperature at three different positions along the probe. Table 1 summarizes the installed sensors, including the quantity of each type of sensor and their corresponding model types.

Table 1 Sensor Summary

| Sensor Type | Sensor Label | Number Installed | Measurements made |
|--|---------------|------------------|--|
| Horizontal asphalt strain gauges | AS-XX-Y-# | 8 | Strain ($\mu\epsilon$) |
| Vertical asphalt strain gauges | VAS-Y-# | 4 | Strain ($\mu\epsilon$) |
| Temperature sensors | TM-XX-# | 7 | $^{\circ}\text{C}$ |
| Moisture probes | MOI-XX-# | 5 | Volumetric Water Content (VWC - m ³ /m ³) |
| Multi-depth deflectometers (MDD) | N/A* | 2 | Depth (in.) |
| Total earth pressure cells (TEPC) | PC-XX-Y-# | 8 | Pascals (MPa) |
| Temperature probes | TEMPS-01/02-# | 2 | $^{\circ}\text{C}$ |

*Not currently installed within the pavement structure at the time of writing.

The sensors were installed within a 10 m test section on Courtland Avenue, with each sensor positioned at a 1-meter interval from one another. Additionally, the sensors were placed 0.7 m away from the pavement edge. The installation design comprised two rows of sensors: a right row closest to the pavement edge, aligning closely with the right wheel path of passing vehicles. Additionally, a left row of sensors was positioned 0.7 m from the right row to capture the tire wander from the right wheel path. They will be referred to as the “right sensor array” and the “left sensor array”, respectively. This configuration is depicted in Figure 2, which also illustrates the types of sensors installed along both rows. Figure 3 showcases the relative depths of the sensors underground and within each pavement layer.

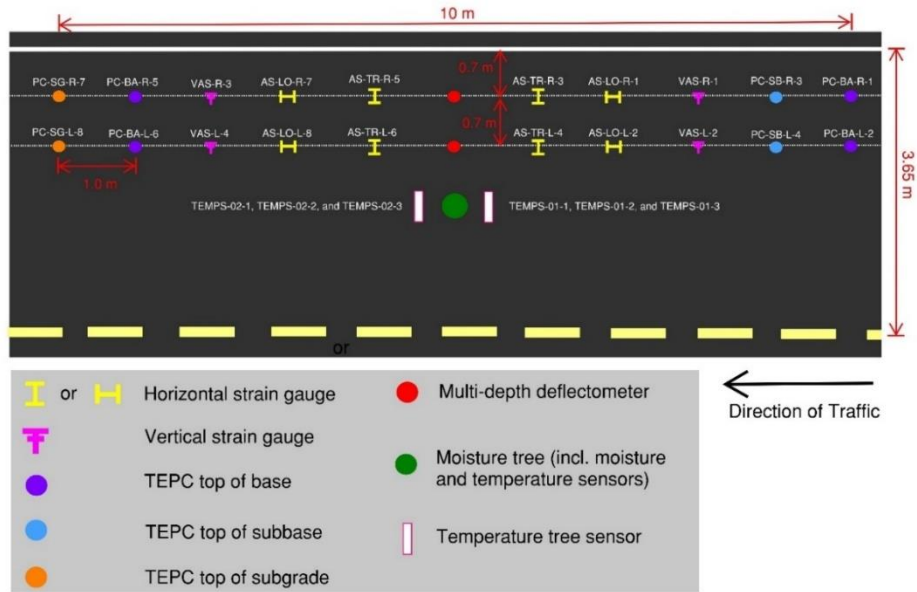


Figure 2 Plan view of the sensor instrumentation scheme.

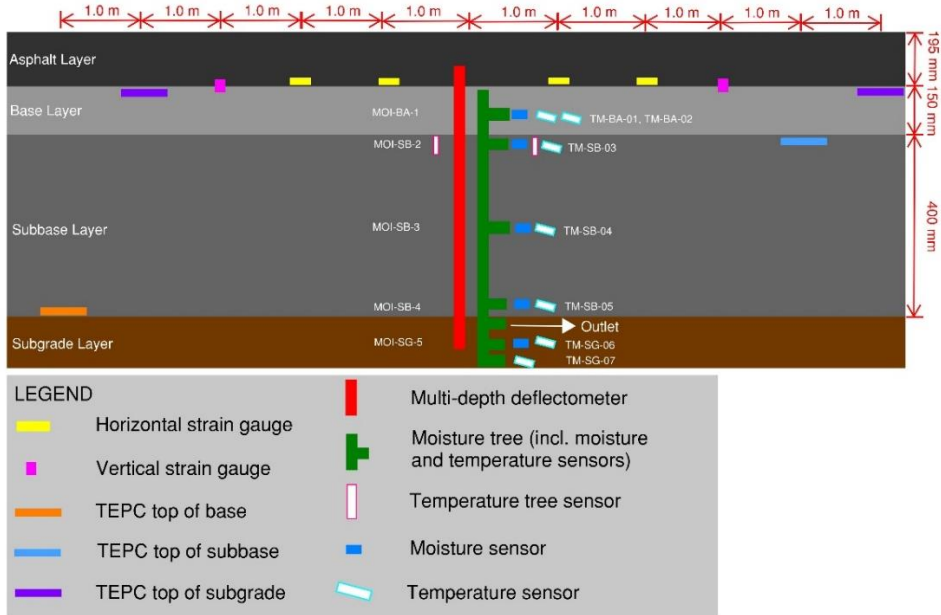


Figure 3 Side view of the sensor instrumentation scheme.

Adjacent to the two rows of sensors positioned between the vehicle wheel paths, an installation called the "moisture tree" is situated. This moisture tree incorporates PVC pipes at various depths, housing both moisture and temperature sensors. The concept of the moisture tree design draws inspiration from previous projects, including the work of Oyeyi (2022), to optimize the installation process for the moisture and temperature sensors. The construction phase becomes more streamlined and efficient by pre-positioning the sensors at the required depths. Moreover, all sensor wires are routed through the moisture tree, ensuring no sensors are inadvertently missed or left unconnected. Table 2 provides detailed information about the depths and specific sensors installed within each hole of the moisture tree.



Figure 4 (a) Moisture tree through which all sensors were threaded, (b) Image showcasing how all the sensors were threaded through the moisture tree, (c) installation of the moisture tree on site.

Table 2 Type and Depth of Sensors in the Pavement Structure

| Opening Number | Location relative to subgrade (mm) (subgrade = 0 mm) | Sensor Name and Location |
|----------------|--|--|
| Hole 1 | 530 | All asphalt strain gauges |
| Hole 2 | 480 | MOI-BA-1; TM-BA-01; TM-BA-02; PC-BA-R-1; PC-BA-L-2; PC-BA-R-5; PC-BA-L-6 |
| Hole 3 | 340 | MOI-SB-2 ; TM-SB-03 ; TEMPS-01-1/2/3; TEMPS-02-1/2/3; PC-SB-R-3; PC-SB-L-4 |
| Hole 4 | 200 | MOI-SB-3; TM-SB-04 |
| Hole 5 | 70 | MOI-SB-4; TM-SB-05 |
| Hole 6 | -70 | Sensor wire outlet |
| Hole 7 | -180 | MOI-SG-5; TM-SG-06; PC-SG-L-8; PC-SG-R-7 |
| Hole 8 | -340 | TM-SG-07 |

Sensor signals are then all sent to the Data Acquisition System (DAS), which contains the necessary technology to store the data produced by the sensors from which the data can be analyzed. It should be noted that after the installation of the sensors, all sensors were tested, and it was discovered that the vertical strain gauges' data was significantly out of range and unresponsive to any loads, indicating possible damage or malfunction. Consequently, these vertical strain gauges were assumed to be broken and excluded from the data collection and analysis. In addition, at the time of writing, the installation of the multi-depth deflectometers (MDD) had not yet been completed. The MDD installation is planned for a future date, allowing for additional data collection and enhanced analysis capabilities.

3.1. Truck Testing Description

To date, two truck tests have been performed to assess the impact of a known load on the response of the sensors. The first truck test, performed in October of 2022, was done to capture the conditions and responses of the pavement right after the asphalt was poured. The second truck test took place five months later, in March 2023. This truck test was done to capture the effects of a known load at lower ambient temperatures. Figure 5 below shows a summary of the two tests.

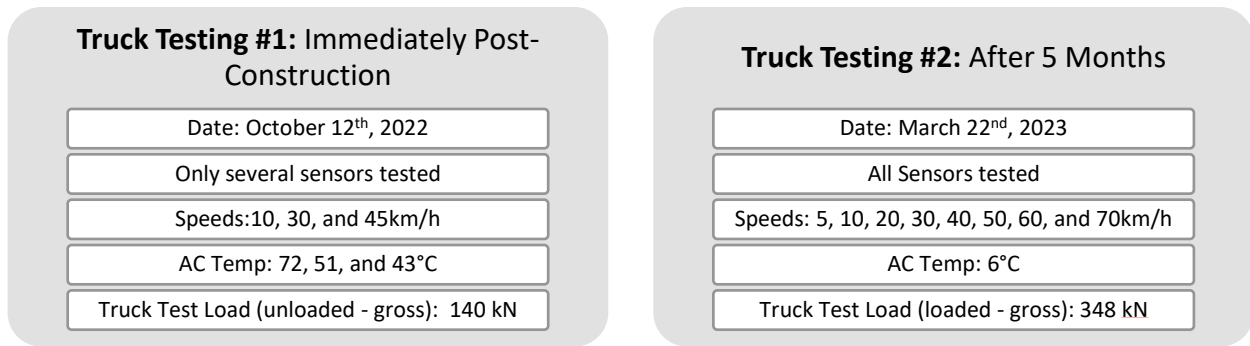


Figure 5 Summary of the details of each truck test, including the date, number of sensors tested, speeds and temperatures tested and the gross weight of the trucks at the time of testing.

The trucks used for the truck testing were typical construction hauling trucks with a steering axle, a middle single axle with dual tires, and a tandem axle with dual tires at the end. Figure 6 showcases an image of this truck.



Figure 6 An image of a truck used for truck testing, with a steering axle, single axle with dual tires and tandem axle with dual tires.

4.0 Results

Based on the two truck tests, results were gathered for all of the load and environmental sensors. In terms of analysis, three major aspects were looked at specifically (Maadani et al., 2015):

1. The effect of speed on layer strain and pressure.
2. The effect of axle load/traffic on layer strain and pressure.
3. The effect of temperature/moisture on layer strain and pressure.

These will be completed through several comparisons of the truck tests.

4.1. Traffic Impact Results – Construction

Only a few sensors could be tested during the post-construction truck testing, as shown in Figure 5, due to the unavailability of the DAS and limited testing equipment. These sensors included a couple of strain gauges and pressure cells. Special attention was given to selecting longitudinal and transverse strain gauges and pressure cells from various depths. Furthermore, temperature and moisture data were also collected.

For the construction phase, the truck test was conducted at three different temperatures: 72°C, 51°C, and 43°C. The truck used for testing was also unloaded and had a gross weight of 140 kN. During testing, the ambient temperature was about 16°C and sunny.

4.1.1. Comparison of Longitudinal and Transverse Strain at 72°C

The initial analysis compared strain variations at different testing speeds (45 km/h, 30 km/h, and 10 km/h). This assessment was conducted across all testing temperatures (72°C, 51°C, and 43°C). Figure 7 presents the results specifically for 72°C. The figure also illustrates the signal response from different axles, a recurring pattern observed in much of the collected data. However, due to considerable variability in the data at this speed and occasional data gaps during collection, the most insightful data pertained to the longitudinal and transverse strain at 45 km/h. Both sensors were positioned in the right sensor array.

One notable finding from this dataset is that the magnitude of longitudinal strain is 63% greater than that of transverse strain for the front tandem axle at 45 km/h. Additionally, the tandem axle exerts the most significant influence on the longitudinal strain. This difference in both strain types is expected. It is likely a result of the anisotropic nature of asphalt, whereby its modulus and strength properties vary in the vertical, longitudinal, and horizontal directions. This property is also the case for the granular unbound layers. It is important to consider in pavement design as traffic loading in the longitudinal directions causes significant anisotropy (Chen et al., 2011).

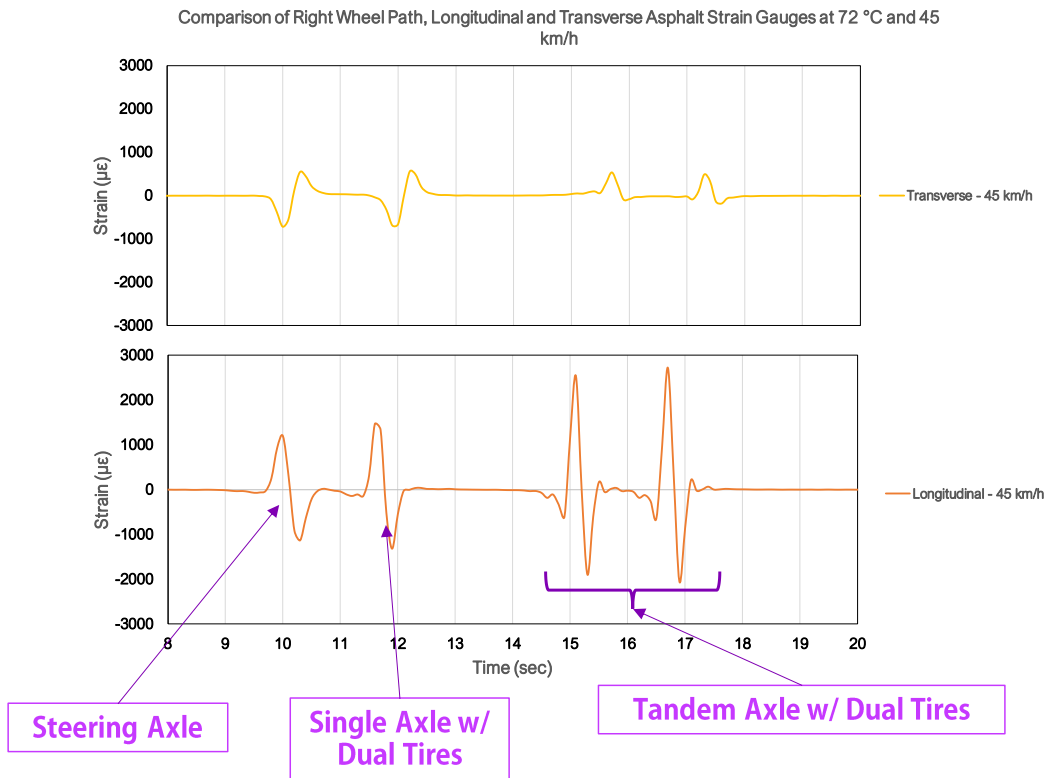


Figure 7 Comparison of the longitudinal and transverse strain responses at 72°C for a truck running at 45 km/h.

4.1.2. Impact of Speed on AC Layer Strain at 51°C and 43°C

Furthermore, the influence of speed on strain was examined at 51°C and 43°C using transverse strain gauges, as illustrated in Figure 8. One trend observed was that at 51°C, a 28% difference in strain magnitude was observed for the front tandem axle when comparing the results at 45 km/h and 30 km/h. The transverse strain for the tandem axle decreased as the speed decreased, with a higher strain at 45 km/h compared to 30 km/h. Conversely, for the steering axle and single axle with dual tires, the strain response at 30 km/h was greater than at 45 km/h.

Typically, in such cases, one would expect that at lower speeds, the wavelengths between axles would be longer (peaks further apart). This trend would apply to all axles since it takes more time for them to pass over any given sensor. However, the opposite trend was observed for the tandem axles. This suggests that material properties may be influencing the results at high temperatures. Another possibility is that the truck consistently passed over the right sensor array more frequently at 45 km/h than at 30 km/h, thereby reducing the wander effect.

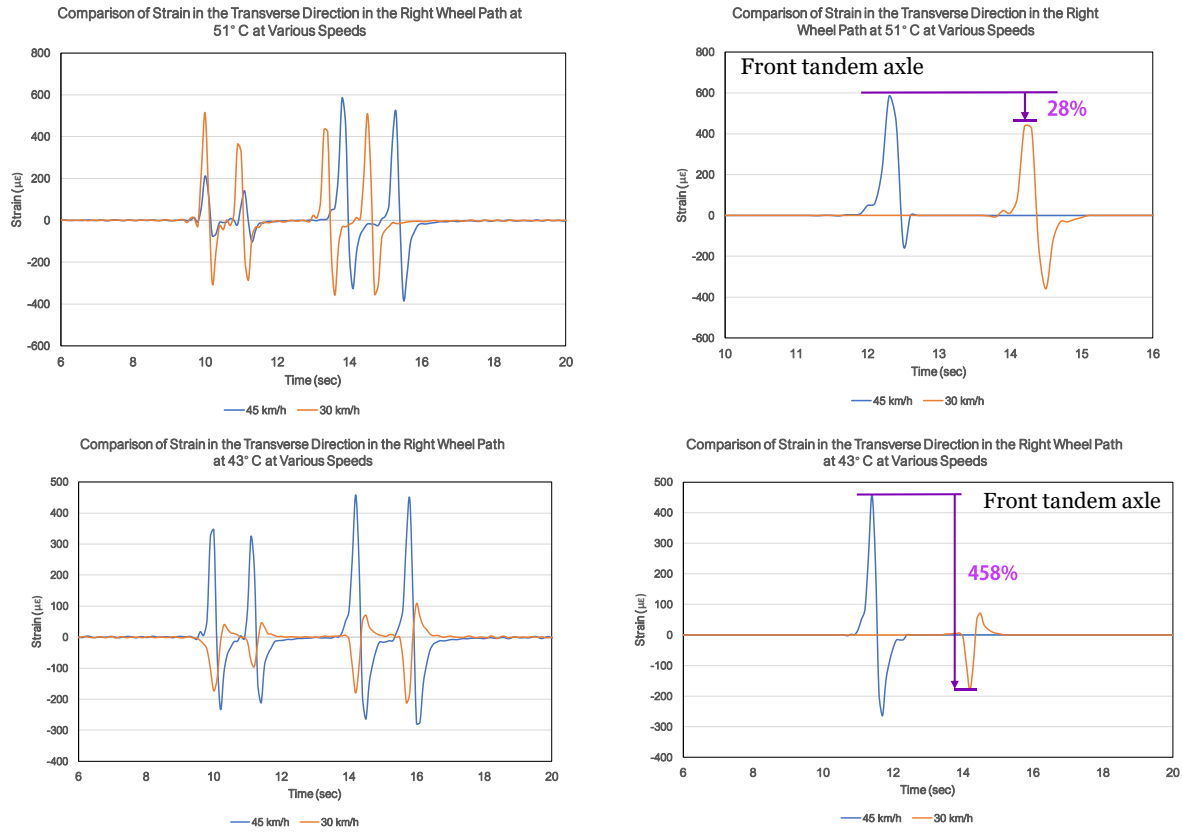


Figure 8 Comparison of the strain response in the transverse direction at 51°C and 43°C, along with close-up comparisons of the front tandem axle at each temperature.

When comparing the results between the temperatures of 51°C and 43°C, it is evident that the results at 51°C exhibit greater severity. Specifically, the strain magnitudes are larger at 51°C than at 43°C. For example, at 51°C, the maximum strain impact reaches nearly 600 µε, whereas, at 43°C, the maximum strain impact ranges between 400 and 500 µε because the AC layer becomes stiffer at cooler temperatures, which means that the pavement will better resist loads, resulting in lower strain values (Sulejmani et al., 2020).

4.1.3. Impact of Speed on Layer Pressure at 51°C and 43°C

Along with determining the impact of speed on layer strain at various temperatures, the impact of speed on layer pressure was performed at various temperatures. For similar reasons, the data at 51 °C and 43 °C will be used in the analysis only. At both temperatures, the study examined the pressure variation in different layers, including the base, subbase, and subgrade, and extracted relevant trends. The results of this analysis are presented in Figure 9.

The primary trend observed is that the magnitude of the pressure impact generated by the passing truck is lower at slower speeds, and this is most clearly the case for the base and subbase layers and all axles. In the

subgrade layer, the impact at both speeds is very similar, suggesting that at high temperatures, the damage imparted on the subgrade layer at various speeds will be similar.

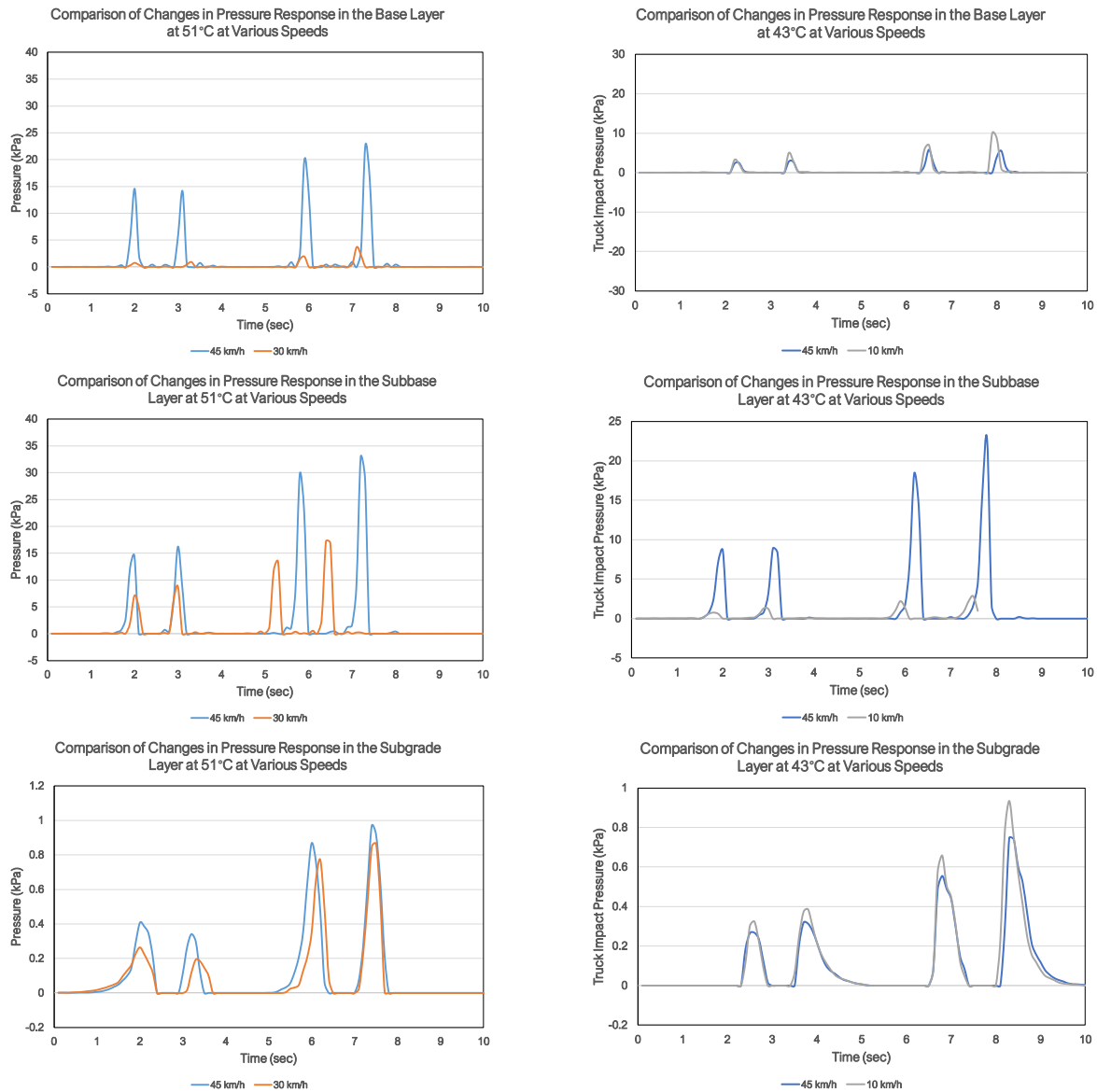


Figure 9 Comparison of the pressure response in the base, subbase and subgrade layers at 51°C and 43°C at various speeds.

In addition, as one goes down the pavement layers, there is a noticeable variation in the magnitude range of the pressures. For instance, in the base, the maximum pressure impact is around 20 kPa. In the subbase, the impact is about 30 kPa; in the subgrade, the impact is around 1kPa. This shows a reduction in subgrade pressure compared with beneath the AC layer (An et al., 2018).

4.1.4. Impact of Temperature on Layer Strain at 45 km/h, 30 km/h and 10 km/h

The subsequent analysis focused on examining the influence of temperature on layer strain and pressure at different speeds. First, the impact of temperature on layer strain was assessed at speeds of 45 km/h, 30 km/h, and 10 km/h to identify trends. Figure 10 displays the strain impacts for a transverse sensor at 45 km/h and 30 km/h.

One noticeable observation is that at higher temperatures, the magnitude of the horizontal strain tends to be larger compared to lower temperatures. For instance, at 45 km/h, the magnitude decrease from 72°C to 51°C is approximately 61%, while the decrease from 72°C to 43°C is around 37%. The greatest horizontal strain occurs at 72°C asphalt concrete temperature. This is expected because the AC layer is softer (Sulejmani, et.al, 2021).

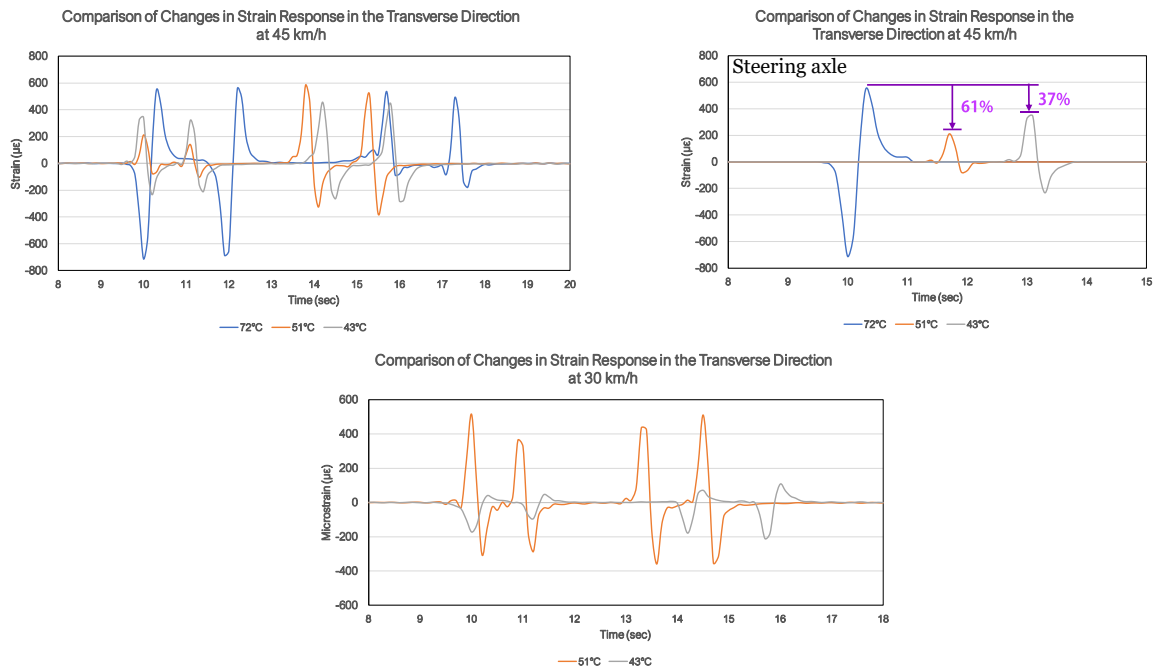
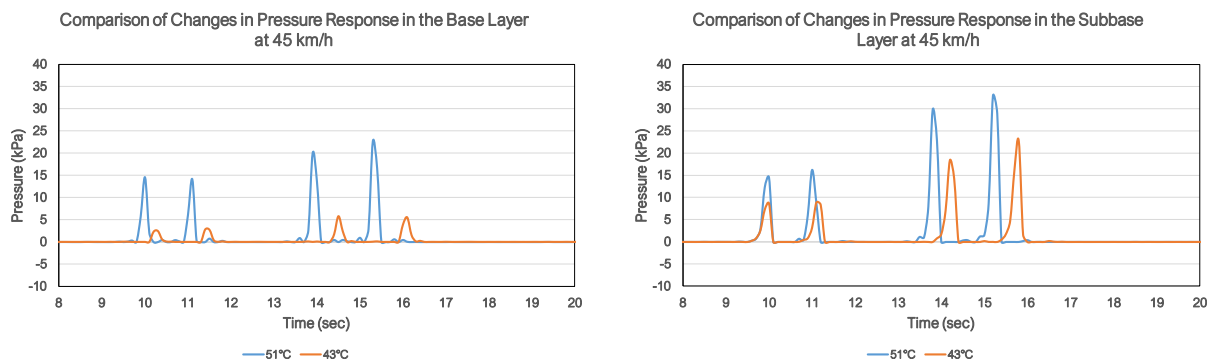


Figure 10 Comparison of the strain response at 45 km/h (top images) and 30 km/h (bottom image).

4.1.5. Impact of Temperature on Layer Pressure at 45 km/h, 30 km/h and 10 km/h

The impact of temperature on layer pressure was also examined for speeds of 45 km/h, 30 km/h, and 10 km/h. Figures 11 and 12 display the results of this analysis. The primary trend observed is that at higher temperatures, the pressure impact is larger compared to lower temperatures. This trend is consistent across all tested speeds (Maadani & Abd El Halim, 2017). Like what was described in Section 4.1.3, when analyzing the pressure response at different temperatures, the magnitude of the pressure impact varies within each layer. For instance, the maximum pressure impact in the base layer is approximately 20 kPa. In the subbase layer, the maximum impact ranges from 30 kPa at 45 km/h to 17 kPa at 30 km/h and around 7 kPa at 10 km/h (An et al., 2018).



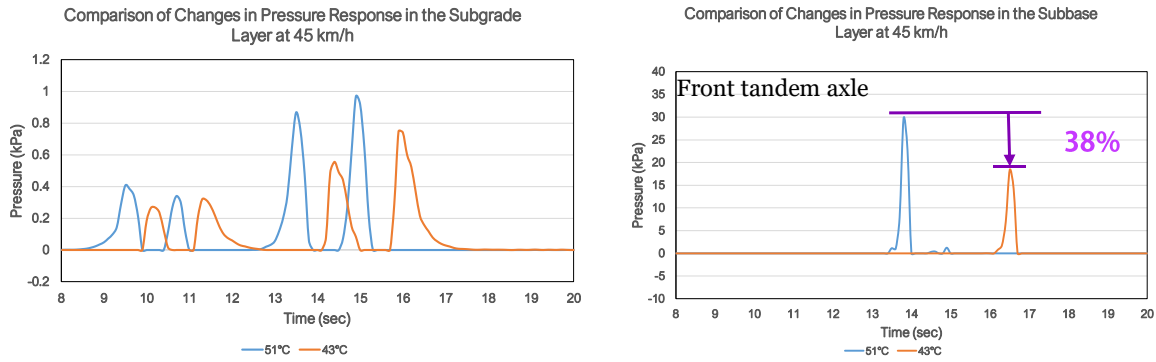


Figure 11 Comparison of the pressure response at 45 km/h in the base, subbase, and subgrade, with further analysis for the front tandem axle in the subbase layer.

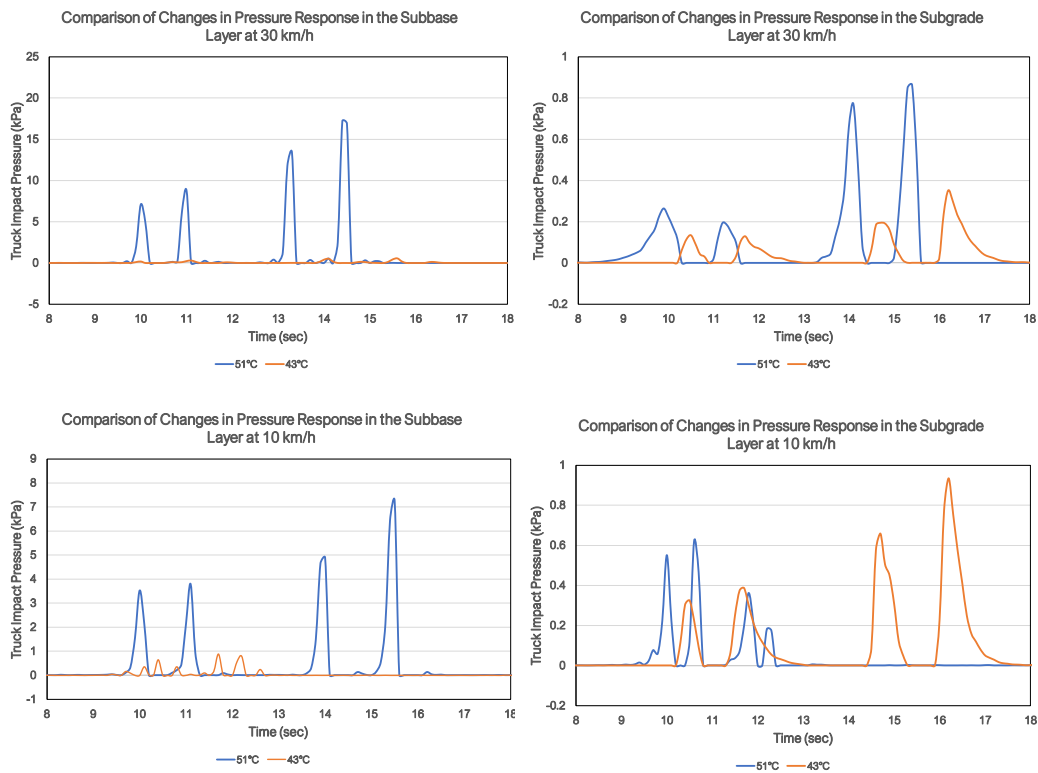


Figure 12 Comparison of the pressure response at 30 km/h and 10 km/h in the base, subbase and subgrade.

4.1.6. Comparison of Pressure in the Pavement Structure during Construction

Figure 13 presents a pressure profile, illustrating the pressure response at various depths within the pavement structure. The pressure profile was generated for temperatures of 51 °C and 43 °C, comparing the same sensor at both temperatures to ensure consistency. Figure 13 shows that the pressure has a lesser impact on the pavement structure at lower temperatures. For example, at 51 °C, the pressure in the base layer is 50% higher than at 43 °C.

While temperature significantly influences the magnitude of pressure impact in the base and subbase layers, there is negligible change in the subgrade layer. The pressure impact in the subgrade layer remains low and relatively constant regardless of the temperature of the asphalt concrete layer. This indicates that during

construction, the subgrade experiences minimal impact, and its behaviour is not significantly affected by the temperature of the asphalt concrete layer.

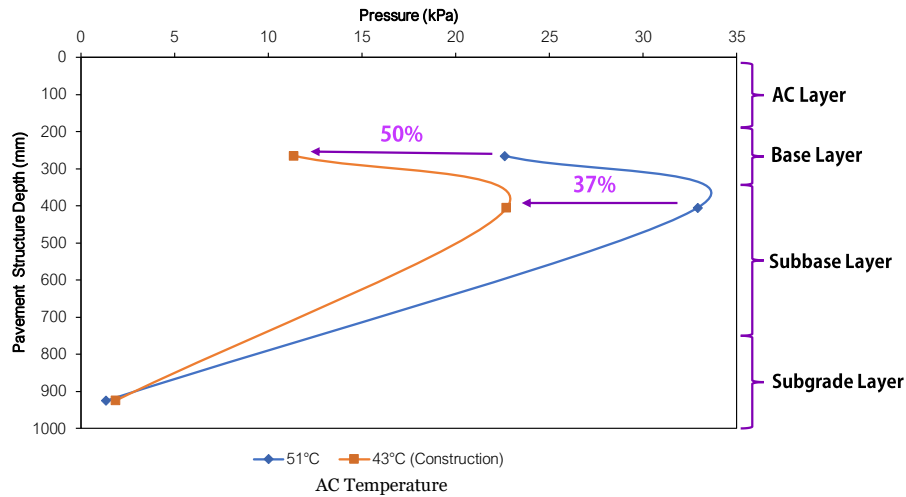


Figure 13 Pressure depth profile indicating changes in pressure during the construction phase at 51°C and 43°C.

4.2. Traffic Impact Results – 5 months Later

The second track testing occurred on March 22nd, 2023, approximately five months after the initial construction truck testing. During this truck testing session, all sensors were successfully tested as the DS (Data System) was operational at that time. Various speeds were examined, including 5, 10, 20, 30, 40, 50, 60, and 70 km/h at an asphalt temperature of 6 °C, while the ambient temperature was about 3 °C. In this truck testing, the truck was loaded and had a gross loading weight of 348 kilonewtons.

4.2.1. Impact of Speed on Longitudinal & Transverse Strain

The primary focus of the analysis for the truck testing conducted five months after construction was to examine the effect of speed on pressure and strain. This section will describe the impact of speed on the longitudinal and transverse strain. Figure 14 illustrates the results of the truck testing at various speeds for both longitudinal and transverse strain.

A significant trend emerges when analyzing the longitudinal strain: the strain decreases with increasing speed. As the speed of the truck rises, the amplitudes between the axle peak responses shorten, and the magnitudes of the strain diminish. This trend is expected because when a truck travels at higher speeds over a pavement structure, the impact that each tire has on each sensor decreases. Additionally, all axles pass over a specific sensor more quickly. This result is corroborated by Liu et al. (2022).

In contrast, a different trend is observed in the transverse direction. As the speed increases, the amplitude between the axle peaks still diminishes due to the truck running at a faster speed, causing all axles to pass over a specific sensor more quickly. However, the magnitude of the strain response increases as the speed rises. This finding also aligns with what was observed in the construction data (see Section 4.1.2).

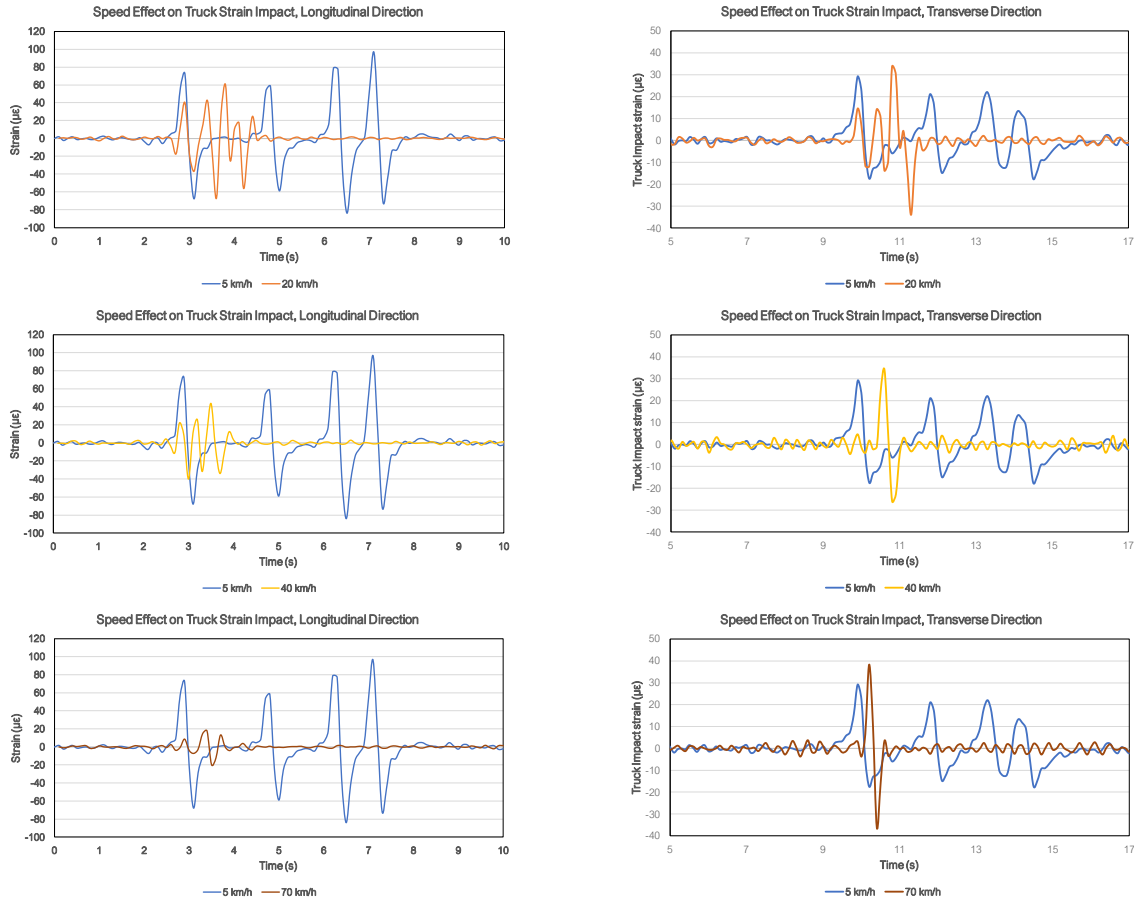


Figure 14 Comparison of the impact of longitudinal (left) and transverse (right) strain at 5km/h and 20, 40 and 70 km/h.

4.2.2. Impact of Speed on Pressure in the Base, Subbase and Subgrade

Figure 15 illustrates the impact of speed on the pressure experienced in the base layer, subbase layer, and subgrade layer of the pavement structure. Overall, a consistent trend is observed across all three layers: as the speed increases, the magnitude of the pressure decreases. However, there are variations within each layer that warrant further analysis.

In the base layer, there are instances where the pressure magnitude at certain speeds (e.g., 20 km/h) is higher than at the lowest tested speed of 5 km/h. For example, the magnitude of the front axle pressure at 5 km/h is approximately 17.6 kPa, whereas, at 20 km/h, it is around 30.1 kPa. This suggests that the impact of the load on the base layer is influenced by speed, with higher speeds resulting in larger pressure magnitudes in some cases. Like the base layer, the subbase layer exhibits a similar trend. Additionally, the magnitudes of the pressure responses in the subbase layer are slightly larger than those in the base layer. This indicates that loads have a greater impact on the subbase layer than the base layer. Finally, the subgrade layer follows a similar trend as demonstrated in the previous two layers, with pressure magnitudes decreasing as speed increases. However, the overall magnitudes of the pressure responses in the subgrade layer are lower. This is expected since the sensors in the subgrade layer are located furthest away from the applied load.

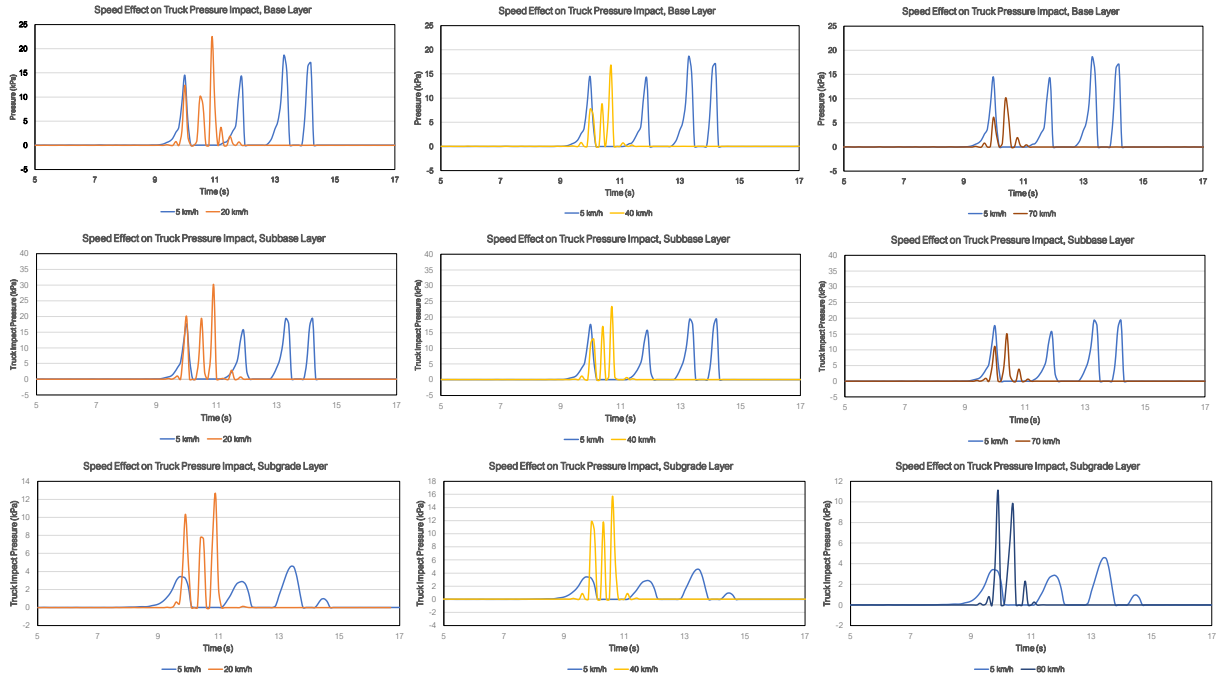


Figure 15 Comparison of the impact of the pressure in the base, subbase and subgrade at 5km/h and 20, 40 and 70 km/h.

4.3. Strain and Pressure Comparison: Construction and 5 Months After

To facilitate a more comprehensive comparison between the impact of loads on the pavement structure during construction and five months after construction, Figure 16 presents graphs depicting the maximum longitudinal and transverse strains and the maximum pressures for each tested temperature, with sufficient and clear data.

Starting with the pressure comparison in Figure 16, the pressure experienced substantial fluctuations during construction, ranging from approximately one to two kilopascals in the subgrade layer to over 30 kPa in the subbase layer. This stark difference highlights the varying levels of pressure experienced by each layer, emphasizing that during construction, the subgrade layer is subjected to less pressure than the base and subbase layers. In contrast, five months after construction, the maximum pressure distribution shows a more evenly distributed load across the pavement structure. While the subgrade layer still experiences the lowest pressure, averaging around 16 kPa, the disparity between the load impact on the subgrade layer and the impact on the subbase and base layers is significantly smaller. This suggests that as the pavement cools and hardens after construction, the load is more effectively transmitted to the subgrade layer.

Another noticeable trend in the transverse strain results, particularly in the bottom-left diagram in Figure 16 depicting maximum transverse strain during the construction phase, is that the strain response at 72°C is lower than that at 51°C and 43°C. One would expect that if the measurement at 51°C yields 714 $\mu\epsilon$, then at 72°C, it should read higher, perhaps around 1000 or 1100 $\mu\epsilon$. This suggests the possibility that the path of the truck's wheels passing over the sensors deviated slightly from directly aligning with the sensors due to wander. It is essential to investigate the relationship between the tire's position and the sensor's response further.

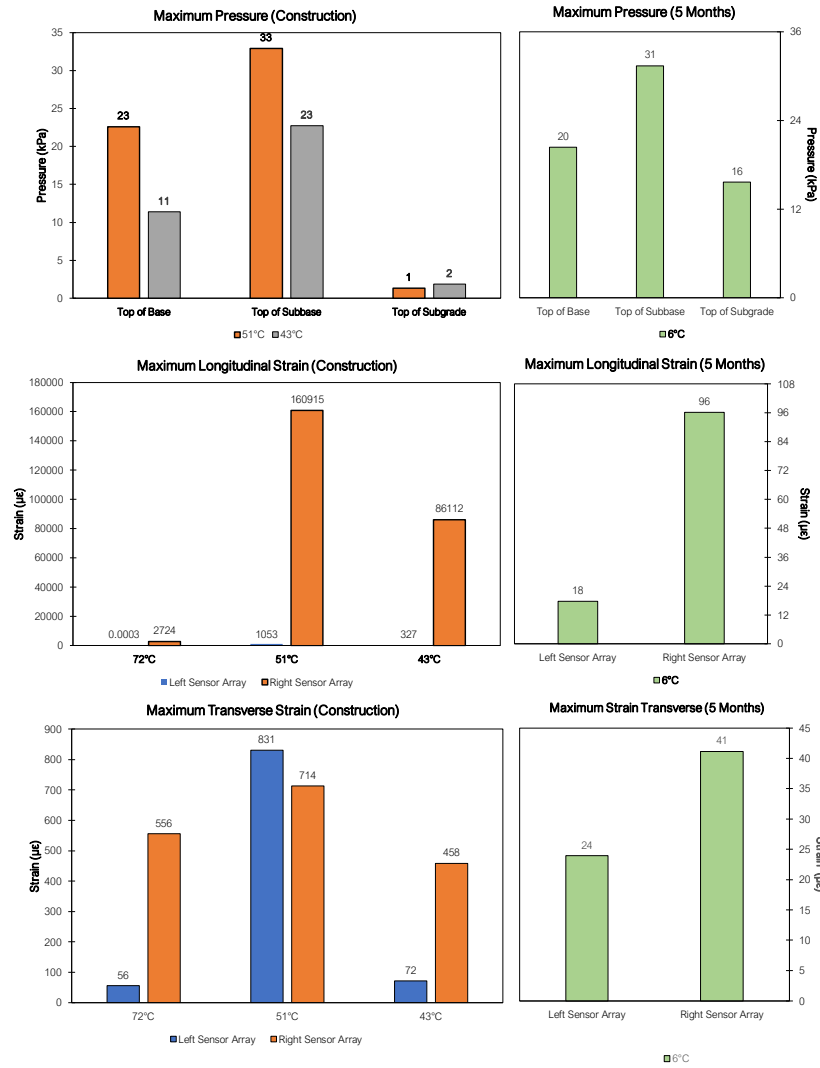


Figure 16 Comparison of the pressure during construction and 5 months after (top) and the transverse and longitudinal strain during construction and 5 months after (middle and bottom).

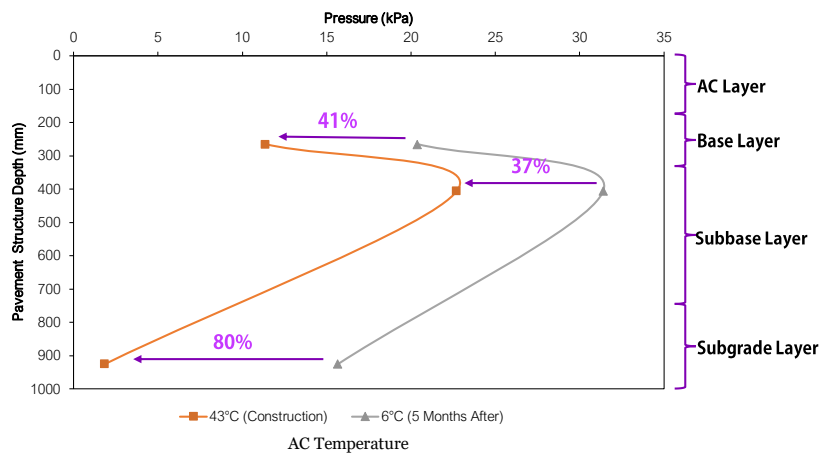


Figure 17 Pressure depth profile showing changes in pressure during the construction phase (43°C) and 5 months after (6°C).

Examining the strain comparison in Figure 16, the most notable observation is that the pavement structure experiences substantial strain impacts during construction. For instance, the maximum longitudinal strain, particularly in the right sensor array, exceeds 160,000 $\mu\epsilon$. In contrast, the measurements obtained five months after construction indicate an average maximum strain of approximately 96 $\mu\epsilon$. This indicates a significant difference between the response conditions during construction and post-construction. Furthermore, it highlights the inconsistency in the data obtained during construction, particularly in comparing the right and left sensor arrays. This indicates variability in the state of the asphalt concrete during construction, resulting in high magnitudes of strain. These higher strains imply that elevated strains may be induced immediately after construction, which is detrimental to the fatigue performance of the pavement (Huang, 2003, MTO, 2013).

Figure 17 compares the pressure depth profile between a sensor during construction at 43 degrees Celsius and the same sensor five months after at six degrees Celsius. The notable observation is that there is an increase in pressure between the construction and in-service periods. This increase can be attributed to the higher traffic load during the testing phase five months after construction (140 kN unloaded vs. 348 kN loaded).

The largest disparity in pressure occurs in the subgrade layer, where there is an approximately 80% difference between the pressure results during construction and the subsequent testing period. This significant increase in pressure indicates the impact of the heavier traffic load during the post-construction phase. It further underscores the importance of considering the actual traffic load and its variation when evaluating the performance of the pavement structure.

4.4. Environmental Results

In addition to analyzing the structural data, environmental data, including moisture and temperature profiles, were collected and examined. The following sections will present the findings related to these environmental factors. The environmental temperature and precipitation data collected was gathered from Environment Canada and was used as it was determined to be statistically significant, as described in Oyeyi (2022).

4.4.1. Hourly Pressure and Strain Profiles

Figures 19 and 20 depict the pressure and strain fluctuations relative to the ambient temperature. The data was collected from March to April 2023. Both figures reveal a daily peak in strain and pressure. The highest pressure impact is observed between 8 and 9 PM, while the lowest occurs around 5 to 6 AM. This suggests a pattern where heavy vehicles tend to pass through the site later in the day to minimize disruption to daily activities and peak traffic hours.

Regarding pressure, the subbase layer, located 405 millimetres below the asphalt surface, experiences the greatest peaking, while the subgrade layer exhibits the least significant cyclical pressure. The pressure profile indicates that as the ambient temperature decreases, the maximum pressure exerted on the pavement section during a 24-hour period increases.

As for strain, a similar daily cyclical trend is observed for strain, with the highest peaking occurring between 9 and 11 AM and the lowest occurring between 5 and 7 PM. Like pressure, as the ambient temperature decreases, the maximum strain variation increases during the daily cycle.

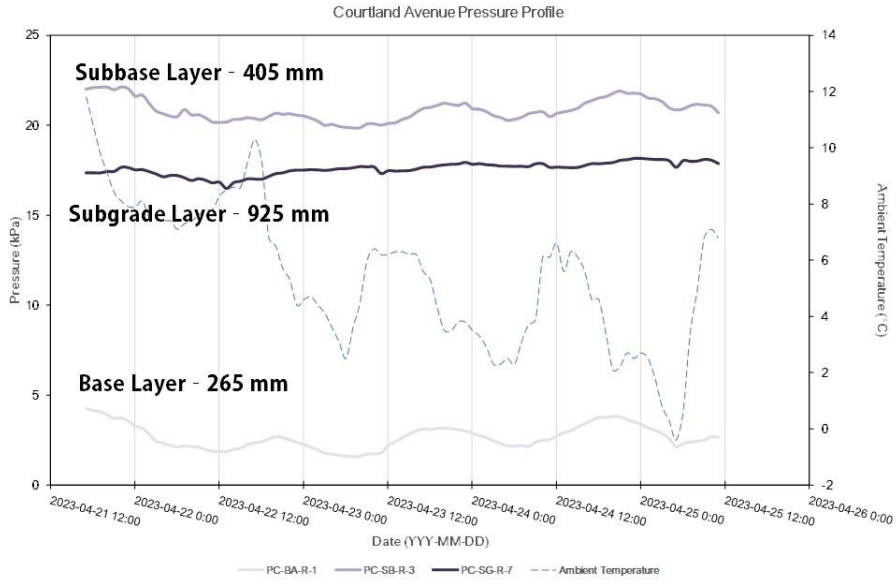


Figure 18 Pressure profile over several days shows the cyclical pressure peaking in all pavement layers and compared to ambient temperature.

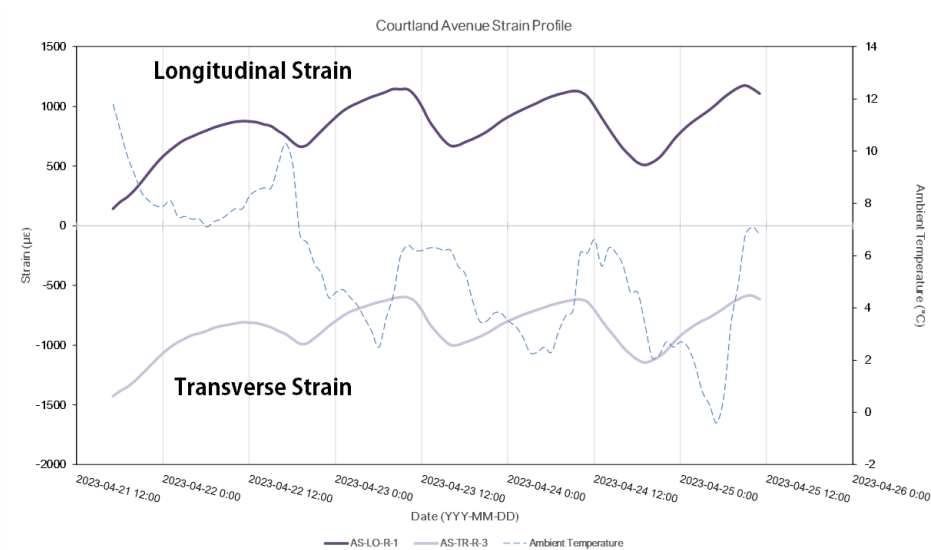


Figure 19 Strain profile over several days shows the cyclical peaking of longitudinal and transverse strain compared to ambient temperature.

4.4.2. Hourly Moisture Profile

The hourly moisture profile was plotted alongside the daily precipitation levels from March to April 2023. The profiles were created for the base layer, three subbase sensors (at different depths – 405 mm, 545 mm and 675 mm), and one subgrade sensor. Despite some missing data due to issues with the data system, there are still discernible trends in the results depicted in Figure 20.

Firstly, as one moves deeper into the pavement structure, the variation in moisture decreases, regardless of the amount of rainfall. This indicates that the moisture content within the layers corresponds to rainfall events. However, further investigation over a longer duration is necessary to obtain a more comprehensive understanding of the moisture trends within the layers.

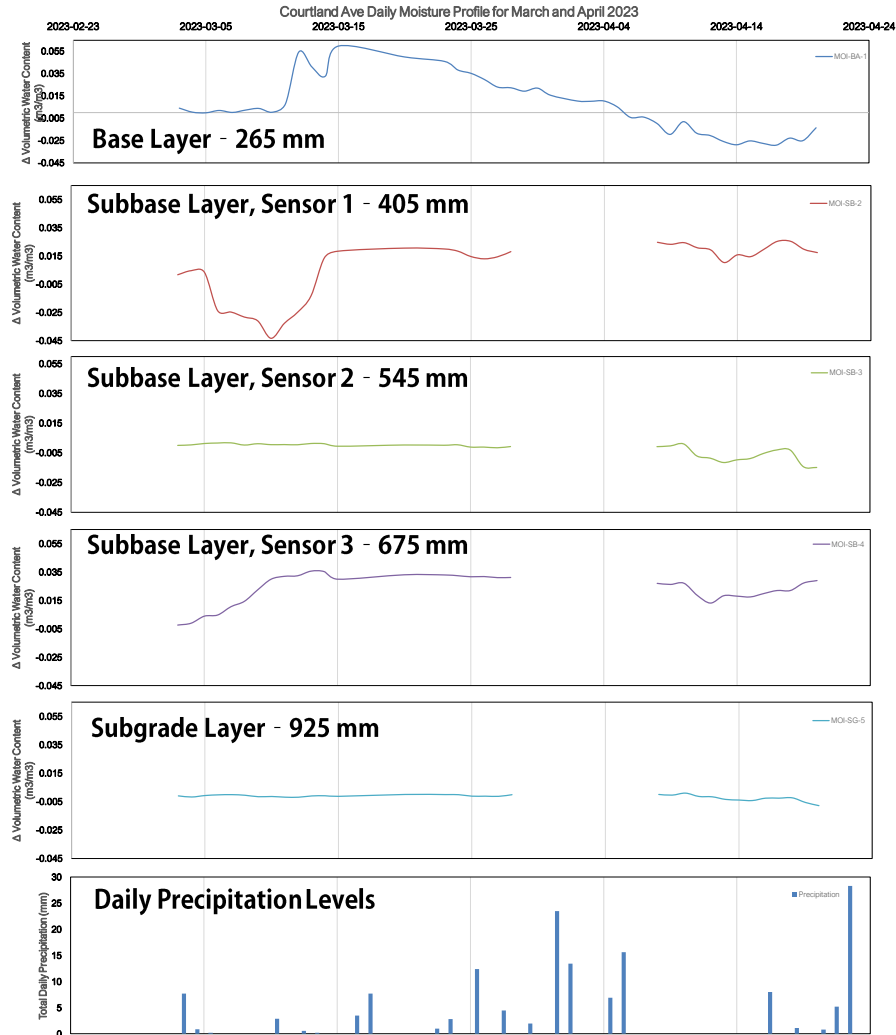


Figure 20 Change in moisture results within each pavement layer (and 3 in the subgrade) compared to ambient precipitation results for Kitchener Waterloo.

5.0 Conclusions and Recommendations

This study used data from a monitored road section in Canada to gather accurate performance and environmental information. The goal was to incorporate this data into the development of an AI model for predicting pavement performance deterioration.

Variations in traffic load level, traffic speed, and layer temperature emerge as significant factors influencing pavements' stress and strain response. Key trends include that strain and pressure results during construction are quite variable and elicit significant strain to the various layers, while after the pavement cools over time, the results are much lower and stable. Moreover, fluctuations in environmental variables like ambient temperature and moisture contribute to variations in the magnitude of stress and strain. Clear trends emerge regarding the impact of temperature increases or decreases on the strain and pressure response. However, the impact of moisture on critical responses requires further evaluation to understand its influence fully. Finally, truck testing has proven to be a valuable method for evaluating pavement response. However, conducting additional assessments over an extended period encompassing different seasons is essential to capture a comprehensive understanding of response trends. This longitudinal evaluation will enable the

identification of patterns and variations in stress and strain over time, improving the accuracy and reliability of pavement performance predictions.

The collected trends and insights are vital for developing an AI model that accurately predicts pavement performance. By considering variations in traffic load, speed, layer temperature, ambient temperature, and moisture, the AI model improves prediction accuracy. This predictive model optimizes pavement design, maintenance strategies, and decision-making, enhancing road infrastructure resilience.

6.0 References

- Amândio, M., Parente, M., Neves, J., & Fonseca, P. (2021). Integration of Smart Pavement Data with Decision Support Systems: A Systematic Review. *Buildings*, 11(12), 579. <https://doi.org/10.3390/buildings11120579>
- An, L., Zhang, F., Geng, Y., & Lin, B. (2018). Field Measurement of Dynamic Compressive Stress Response of Pavement-Subgrade Induced by Moving Heavy-Duty Trucks. *Shock and Vibration*, 2018, 1–12. <https://doi.org/10.1155/2018/1956906>
- Benedetto, A., & Pensa, S. (2007). Indirect diagnosis of pavement structural damages using surface GPR reflection techniques. *Journal of Applied Geophysics*, 62(2), 107–123. <https://doi.org/10.1016/j.jappgeo.2006.09.001>
- Chen, J., Pan, T., & Huang, X. (2011). Numerical investigation into the stiffness anisotropy of asphalt concrete from a microstructural perspective. *Construction and Building Materials*, 25(7), 3059–3065. <https://doi.org/10.1016/j.conbuildmat.2011.01.002>
- Duong, N. S., Blanc, J., Hornych, P., Menant, F., Lefeuvre, Y., & Bouveret, B. (2018). Monitoring of pavement deflections using geophones. *International Journal of Pavement Engineering*, 21(9), 1103–1113. <https://doi.org/10.1080/10298436.2018.1520994>
- Hou, Y., Li, Q., Zhang, C., Lu, G., Ye, Z., Chen, Y., Wang, L., & Cao, D. (2020). The State-of-the-Art Review on Applications of Intrusive Sensing, Image Processing Techniques, and Machine Learning Methods in Pavement Monitoring and Analysis. *Engineering*, 7(6). <https://doi.org/10.1016/j.eng.2020.07.030>
- Huang, Y. H. (2003). *Pavement analysis and design*. Prentice Hall ; London.
- Kang, J. (2022). *Pavement Performance Prediction Using Machine Learning and Instrumentation in Smart Pavement* [PDF]. <https://uwspace.uwaterloo.ca/handle/10012/18752>
- Liu, Z., Gu, X., Ren, H., Zhou, Z., Wang, X., & Tang, S. (2022). Analysis of the dynamic responses of asphalt pavement based on full-scale accelerated testing and finite element simulation. *Construction and Building Materials*, 325, 126429–126429. <https://doi.org/10.1016/j.conbuildmat.2022.126429>
- Maadani, O., Abd El Halim, A. O., & Mostafa, N. (2015). Instrumentation for Monitoring Pavement Performance in Cold Regions. *Journal of Cold Regions Engineering*, 29(4), 04014017. [https://doi.org/10.1061/\(asce\)cr.1943-5495.0000087](https://doi.org/10.1061/(asce)cr.1943-5495.0000087)
- Maadani, O., & Abd El Halim, A. O. (2017). Impact of Asphalt Concrete Temperature and Traffic Loading Speed on Structural Behavior of Flexible Pavement. <https://www.tac-atc.ca/en/conference/papers/impact-asphalt-concrete-temperature-and-traffic-loading-speed-structural-behavior-flexible-pavement>
- Marcelino, P., de Lurdes Antunes, M., Fortunato, E., & Gomes, M. C. (2019). Machine learning approach for pavement performance prediction. *International Journal of Pavement Engineering*, 22(3), 341–354. <https://doi.org/10.1080/10298436.2019.1609673>
- Ministry of Transportation Ontario (2013) *Pavement Design and Rehabilitation Manual*, Materials Engineering and Research Office. Downsview, Ontario
- OECD. (2020). *Transport Bridging Divides*. In *OECD Urban Studies*. OECD. <https://doi.org/10.1787/55ae1fd8-en>
- Oyeyi, A. (2022). *Lightweight Cellular Concrete as Flexible Pavement Subbase Material: Field Performance and Sustainability Study* [PDF]. <http://hdl.handle.net/10012/18938>
- Sulejmani, P., Said, S., Agardh, S., & Ahmed, A. (2020). Impact of temperature and moisture on the tensile strain of asphalt concrete layers. *International Journal of Pavement Engineering*, 22(13), 1–9. <https://doi.org/10.1080/10298436.2020.1715404>